JOURNAL OF MATERIALS SCIENCE 29 (1994) 3062–3070

The role of microstructure on the fracture toughness and fracture behaviour of rubber-reinforced acrylics

R. G. HILL
Department of Material Science and Technology, University of Limerick, Plassey Technology Park, Limerick, Ireland

The influence of microstructure on the fracture toughness, unnotched fracture strength, Young's modulus and fracture mechanism of polybutadiene-reinforced poly(methylmethacrylate)s was investigated. The Young's modulus increased with the degree of dispersion of the polybutadiene phase. A core–shell microstructure with fine ($\simeq$ 1 μm) rubber particles gave the highest fracture toughness. Cavitation of the polybutadiene phase was the dominant toughening mechanism with the particulate rubber morphologies, although additionally localized plastic yielding was observed on the fracture surface of the material with a core–shell microstructure. The material with a lamellar-type rubber morphology exhibited a high fracture toughness as a result of the rubber phase redirecting the propagating crack to produce a rough fracture surface.

1. Introduction

Conventional dough moulded poly(methylmethacrylate) denture base materials and orthopaedic bone cements are prone to brittle fracture.

Acrylic dentures are prone to fracture when dropped or during accidents [1, 2]. Whilst a denture has a non-structural role unlike a bone cement, fragments of fractured denture are often ingested with often disastrous consequences for the person concerned. The upper denture is particularly susceptible to a midline fracture arising from the frenal notch, shown in Fig. 1, which acts as a sharp stress-concentration site for the initiation of fracture.

Brittle fracture of acrylic bone cements is even more important. Weber and Charnley [3] reported a cement fracture rate of 41% for patients with bilateral hip implants. They postulated the cause of fracture as being the "end-bearing effect" arising from the prosthesis loosening in the cement mantle, resulting in the distal part of the cement, becoming loaded in tension and leading to fracture. Clinical fracture of bone cements is now well documented [4–6] and is still a significant cause of failure in total hip replacement procedures. The fracture toughness of acrylic bone cements and denture base acrylics have been studied extensively and the fracture toughness of acrylic bone cements has been recently reviewed by Lewis [7].

Improvements can be made to orthopaedic bone cements in two distinct ways:

(i) minimizing the chance of loosening in the joint, which is the ultimate cause of failure in the cement;

(ii) improving the fracture toughness of the cement in order to prevent fracture.

Only the latter approach is relevant to denture base acrylics.

Loosening may be reduced by minimizing the exotherm that occurs on setting [8] which causes local bone necrosis, or by improving stress transfer in the joint by careful design of the prosthesis or by using polyalkenoate cements that can bond chemically to bone and to the prosthesis [9, 10]. Such cements are currently being actively developed in the UK and in Germany.

Considerable effort has been directed at improving the fracture toughness of acrylic bone cements and denture bases by incorporating fibres [11–15]; however, relatively little attention has been directed towards rubber toughening [16]. This method involves improving the toughness of a glassy polymer by incorporating a polymer with a much lower glass transition temperature; such rubber-reinforced polymers are designed to give optimum toughness, whilst retaining the stiffness of the original polymer [7]. The objective of the present study was to determine the influence of rubber microstructure on the fracture behaviour and failure mechanism of six polybutadiene-reinforced poly(methylmethacrylate)s.

1.1. Theories of rubber reinforcement

Glassy thermoplastic polymers such as polystyrene (PS), styrene–acrylonitrile (SAN) and poly(methylmethacrylate) (PMMA) have all been alloyed or blended with polybutadiene rubbers to give new materials with much greater impact toughness. These toughened polymers characteristically undergo significant stress whitening at the crack tip during fracture. The stress whitening is associated with the

0022–2461

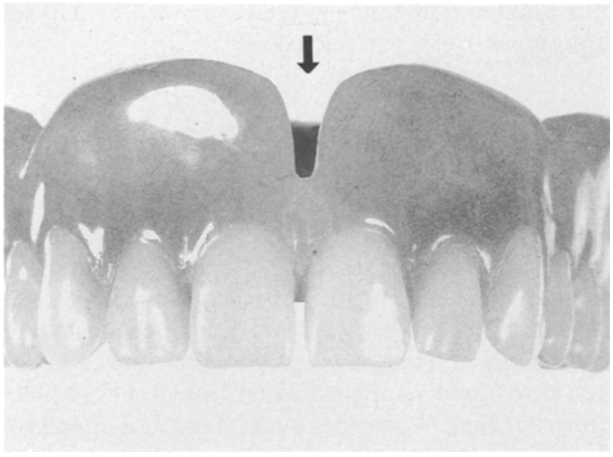

Figure 1 A Frenal notch (arrow) in an upper denture.

toughening mechanism and the amount of stress whitening and toughness enhancement achieved depends critically on the rubber morphology.

The polybutadiene forms a distinct phase, separate from the glassy phase in all these rubber-toughened polymers. There is known to be an optimum size of rubber particle; for example, with high-impact polystyrene (HIPS), rubber particles of the order of 3 μm are known to give optimum toughness, whilst with acrylonitrile–butadiene–styrene (ABS) and rubber-toughened poly(methylmethacrylate) (RTPMMA), much smaller particles less than 1 μm are effective in toughening. Early theories of rubber-toughened polymers concentrated on HIPS and emphasized the importance of crazing. Bragaw [18] proposed that the rubber particles had to be larger than the craze dimensions of the original glassy polymer. It was known that with HIPS and ABS, a bimodal rubber particle size gave optimum toughness and this was explained on the basis of small particles being able efficiently to initiate crazing, whilst larger particles were required to terminate crazes. This view assumes that long crazes are weaker than short crazes, which will not be the case for polymers in which craze thickening occurs by a surface drawing mechanism [19]. Furthermore, microscopy studies [20] have failed to observe any craze termination by rubber particles.

Another mechanism thought to be important was shear-band formation and it was believed that rubber particles initiated shear-band formation in polymers such as ABS. Bucknall and Drinkwater [21] developed a method for distinguishing between crazing and shear-band formation by separating the volume changes due to crazing and the lateral contractions due to shear deformation.

More recently, the importance of cavitation of rubber particles has become appreciated and this is now recognized as causing stress whitening and toughening in many polymers [22, 23]. Haaf *et al.* [23] demonstrated that in ABS and rubber-toughened PVC, stress whitening was associated with cavities aligned at 55°–64° to the stress direction or along the shear bands, and thus Bucknall and Drinkwater's estimates of the relative importance of shear yielding and crazing in ABS are now questionable. In more recent studies, Bucknall *et al.* [24] have also emphasized the role of cavitation and fibrillation of the rubber phase in a number of polymers. Donald and Kramer [25] have also found evidence of rubber fibrillation in HIPS in addition to crazing and their studies of a particulate ABS [26] again showed largely fibrillation and cavitation of the rubber phase followed by localized yielding between particles with small (≈ 1 μm) solid rubber particles and they observed crazing and cavitation with larger ($\simeq 1.5$ μm) occluded rubber particles. When an occluded particle is strained the rubber elongates, whilst the glassy polymer inclusions remain essentially undeformed because of their much higher value of Young's modulus. The rubber locally breaks up into fibrils, but because the rubber is present only as a thin layer around a central glassy inclusion, no large voids are formed. Thus as cavitation and fibrillation of the rubber phase occurs, no harmful cracks are formed within the stress-whitened zone at the crack tip.

Most rubber particles in successfully toughened glassy polymers contain inclusions of the glassy phase and the internal structure of the rubber particles can be very complex, with frequently a core–shell, or cellular structure being present. The exact size of the rubber particles, the amount of occluded glassy polymers they contain and the internal microstructure are very dependent on the polymerization conditions, particularly the degree of shear at the phase inversion point.

Another requirement for obtaining a toughened polymer is that there should be good adhesion between the rubber particles and the matrix [27]. Voids, or glass beads incorporated into glassy matrices are not effective in improving the toughness [28]. In practice, adhesion between the glassy matrix and the rubber is often achieved by grafting the glass matrix polymer chains to the rubber phase to form a block copolymer interface. It is not generally appreciated that the extent of grafting may well influence the toughening mechanisms that operate and the final toughness achieved. For example, the grafted copolymer may well influence the glass transition temperature of the rubber phase and the rubber particle size, because it effectively also acts as a surfactant. Furthermore, if there is a lot of grafting and high shear rates during polymerization, it is possible to produce a lamellar rubber morphology, as opposed to the conventional particulate morphologies. Whilst particulate morphologies are found with most rubber-toughened polymers, some ABS polymers have a lamellar morphology and the influence of this type of morphology on the toughening mechanism has not been considered in the literature to date.

1.2. Fracture of rubber-reinforced polymers

In recent years, our understanding of the fracture process in polymers has come from the development of two distinct approaches. The first approach is the

quantitative measurement of fracture toughness in terms of fracture surface energy, for example Benbow and Roesler [29] and Berry [30], and more recently with a linear elastic fracture mechanics (LEFM) approach, for example Van der Boogart and Turner [31] and Marshall *et al.* [32]. The second approach is to study craze size and shape and its relation to crack propagation. The LEFM approach is used in this paper. This approach has been applied widely to rubber-toughened thermoset polymers such as butadiene acrylonitrile-reinforced epoxy resin [33]. The application of LEFM to rubber-reinforced thermoplastics has been more limited. There is often considerable plastic flow at the crack tip in rubber-reinforced polymers [34] violating one of the assumptions on which LEFM is based. There have been a few attempts to apply non-linear elastic fracture mechanics using the concept of crack opening displacement [35] and contour integral [36]. These concepts have been reasonably successful when applied to toughened thermoplastics. However, the simplicity of the LEFM approach makes its use desirable. The rubber-toughened acrylics studied here are weakly cross-linked with ethylene glycol dimethacrylate, so consequently it is reasonable to attempt to analyse them using an LEFM approach.

2. Experimental procedure

2.1. Preparation of rubber-toughened acrylics

The rubber chosen for this study was a synthetic polybutadiene rubber with a molecular weight of about 50 000 obtained from ISR (Southampton, UK). It was chosen because of its similarity to the rubbers used to toughen high-impact polystyrene (HIPS).

The polybutadiene was dissolved in methylmethacrylate monomer along with 1% by weight benzoyl peroxide. This solution was then suspension-polymerized to produce a fine poly(methylmethacrylate) powder, the particles of which contained the polybutadiene rubber.

Controlling the shear rate in the suspension-polymerization reactor enabled the microstructure of the rubber phase to be varied. Careful choice of reactor conditions enabled six distinctly different rubber morphologies to be produced.

In addition, a homopolymer suspension-polymerized poly(methylmethacrylate), obtained from Cole Polymers (Croydon, UK), was included in the tests.

Samples for testing were prepared by mixing the suspension-polymerized powder with methylmethacrylate monomer containing 10% wt/wt cross-linking agent ethylene glycol dimethacrylate in the ratio of 2:5:1 by weight. The resulting dough was packed in moulds and then polymerized for 14 h at 70 °C and finally for 1 h at 100 °C.

2.2. Determination of microstructure

Small samples of polymerized material were sectioned with an LKB ultramicrotome. It was found that a glass knife angle of 8° enabled sections to be cut prior to staining. The cut sections were stained using 1% osmium tetroxide and then examined by AEI 6B transmission electron microscopy.

2.3. Testing procedures

2.3.1. Double torsion test

Double torsion specimens 65 mm × 40 mm × 3 mm (Fig. 2) were produced in the form of rectangular plates. A vee-notch was made at one end of the specimen and a sharp groove was cut down the centre of the plate approximately 0.5 mm deep using a diamond flitting wheel. The specimens were precracked in the test jig by loading applied by an Instron 1185 Model (Instron, High Wycombe, Bucks, UK) at a crosshead speed of 1 mm min^{-1} with rapid unloading once the crack had started to propagate.

During the test, the specimen was supported on two parallel rollers of 3 mm diameter and 30 mm apart. The load was applied at a constant rate to the vee-notched end of the specimen via two 3 mm diameter ball bearings spaced 10 mm apart. The specimen was therefore subjected to four-point bend loading during which the crack initiated and propagated along the centre of the crack specimen within the groove.

2.3.1.1. Determination of the stress intensity factor. In a double torsion test, the mode I stress intensity factor, K_I, is independent of crack length and is given by Kies and Clark [37] as

$$K_I = PW_m\left[\frac{3(1+\gamma)}{Wt^3t_n}\right]^{1/2} \quad (1)$$

where W_m is the moment arm, W the specimen width, t the specimen thickness, t_n the specimen thickness in the plane of the crack, and γ Poisson's ratio. Values for K_{IC} were obtained for continuous fracture by substituting the load at fracture, P_c, and specimen dimensions into the above equation. A typical load–displacement record for a specimen undergoing stable crack growth is shown in Fig. 3.

2.3.2. Compact tension test

The test and geometry used is based on BS 5447 [38] and has been described previously [39]. Two different thicknesses of specimens (3 and 6 mm) were tested.

2.4. Three-point bend test

The Young's modulus, E, and unnotched fracture strength, σ_f, of each material were determined using

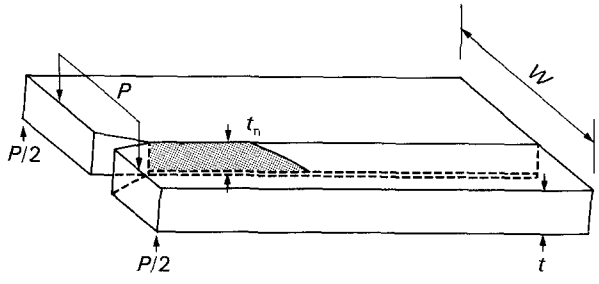

Figure 2 A double torsion testpiece.

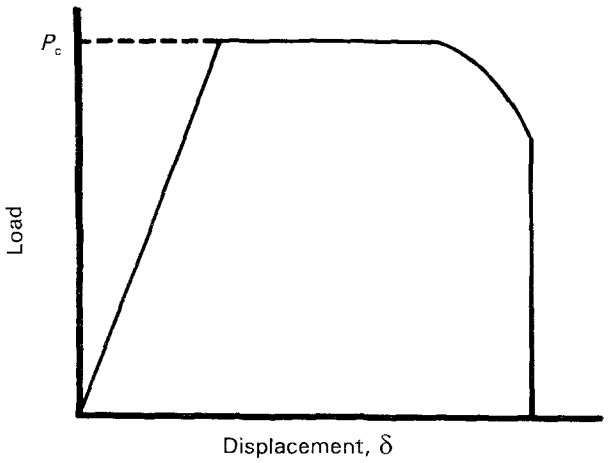

Figure 3 A typical load–displacement record for a double torsion specimen.

a three-point bend test performed with an Instron mechanical testing machine model 1185. The relationship between the applied load, P, and the displacement at the centre of the specimen, δ, for specimens of rectangular cross-sectional area is given by

$$P = \frac{4EWt^3\delta}{L^3} \quad (2)$$

where t is the thickness of the specimen, W the width of the specimen, and L the distance between the supports.

The test was carried out in accordance with ASTMS D790-71 [40]. A span of 50 mm was used with a specimen size of 65 mm × (10 mm ± 0.03) × (3 mm ± 0.03).

Young's modulus was determined from the initial slope of the plot of P against δ.

The unnotched fracture strength, σ_f, is given by

$$\sigma_f = \frac{3P_cL}{2Wt^2} \quad (3)$$

2.5. Calculation of the flaw size

A linear elastic fracture mechanics approach was used to calculate the inherent flaw size, a^*. This value estimates the size of microstructural features, or defects which limit the strength of the material in the absence of an external crack. Actual flaws larger than this size will reduce the strength of the material.

The method used for the calculation of the flaw size is based on the Irwin relation which is applicable to the geometry and loading of a bend-type single-edge notch specimen used by Brown and Strawley [41]

$$K_{IC} = \frac{Y6M}{tW^2a^{1/2}} \quad (4)$$

where M is the bending moment equal to $PS/4$, a is the crack length and Y is a geometrical calibration factor, which in the absence of an external flaw or crack assumes a value of 1.93.

The Irwin relationship can be rewritten in terms of K_{IC}, the unnotched fracture strength and the flaw size

$$a^* = \frac{(K_{IC})^2}{(Y\sigma_f)} \quad (5)$$

2.6. Scanning electron microscopy of fracture surfaces

Fracture surfaces taken from double torsion and compact tension specimens were examined in a stereoscan electron microscope. The surfaces were prepared for examination by depositing a thin layer of gold–palladium alloy on the surface. A silver colloid was applied to the side of the samples to conduct heat away from the fracture surface.

3. Results and discussion

Fig. 4a–f show the microstructure of the polybutadiene rubbers in the six materials prepared. In material A (Fig. 4a) the rubber appears as the dark phase after staining with osmium tetroxide. It is seen that the rubber forms a continuous phase in which are found inclusions of poly(methylmethacrylate). This material has not undergone the phase inversion process to give a polybutadiene phase dispersed in a poly(methylmethacrylate) matrix. Material B (Fig. 4b) has undergone phase inversion (as have all the other materials) to give large multicellular rubber particles with glassy inclusions, dispersed in a glassy matrix. Material C (Fig. 4c) consists of polybutadiene particles aggregated in twos or threes with each particle having a single glassy occlusion. Material D consists of single well-dispersed polybutadiene particles each with a glassy inclusion. This material has the classic "core–shell" microstructure. In material E, the particles are breaking up to form lamellae and material F consists entirely of rubber lamellae. These latter types of microstructure have received very little attention in the literature despite being the basis of some types of commercially available ABS.

Table I shows the data for the Young's modulus and flexural strength for each material. The Young's modulus of all the rubber-reinforced materials is significantly lower than that of the material without any rubber (material G). There is a correlation between the degree of dispersion of the polybutadiene rubber in the poly(methylmethacrylate) phase and the Young's modulus.

The lowest Young's modulus is found with the material where the rubber forms the continuous phase, and the highest modulus is found for the material with fine well-dispersed rubber particles.

The data for the fracture toughness, K_{IC}, are shown in Fig. 5 for both the double torsion (DT) and 3 mm

TABLE I Young's moduli and unnotched fracture strength measured in three-point bending

Material	E (MN m^{-2})	S.D. (n = 10)	σ_f (MN m^{-2})	S.D. (n = 10)
A	1102	86	39.20	3.04
B	1119	113	41.19	4.90
C	1594	118	52.83	3.63
D	2237	79	79.05	3.79
E	1656	40	65.71	1.94
F	1497	104	60.64	3.12
G	2676	89	107.22	6.35

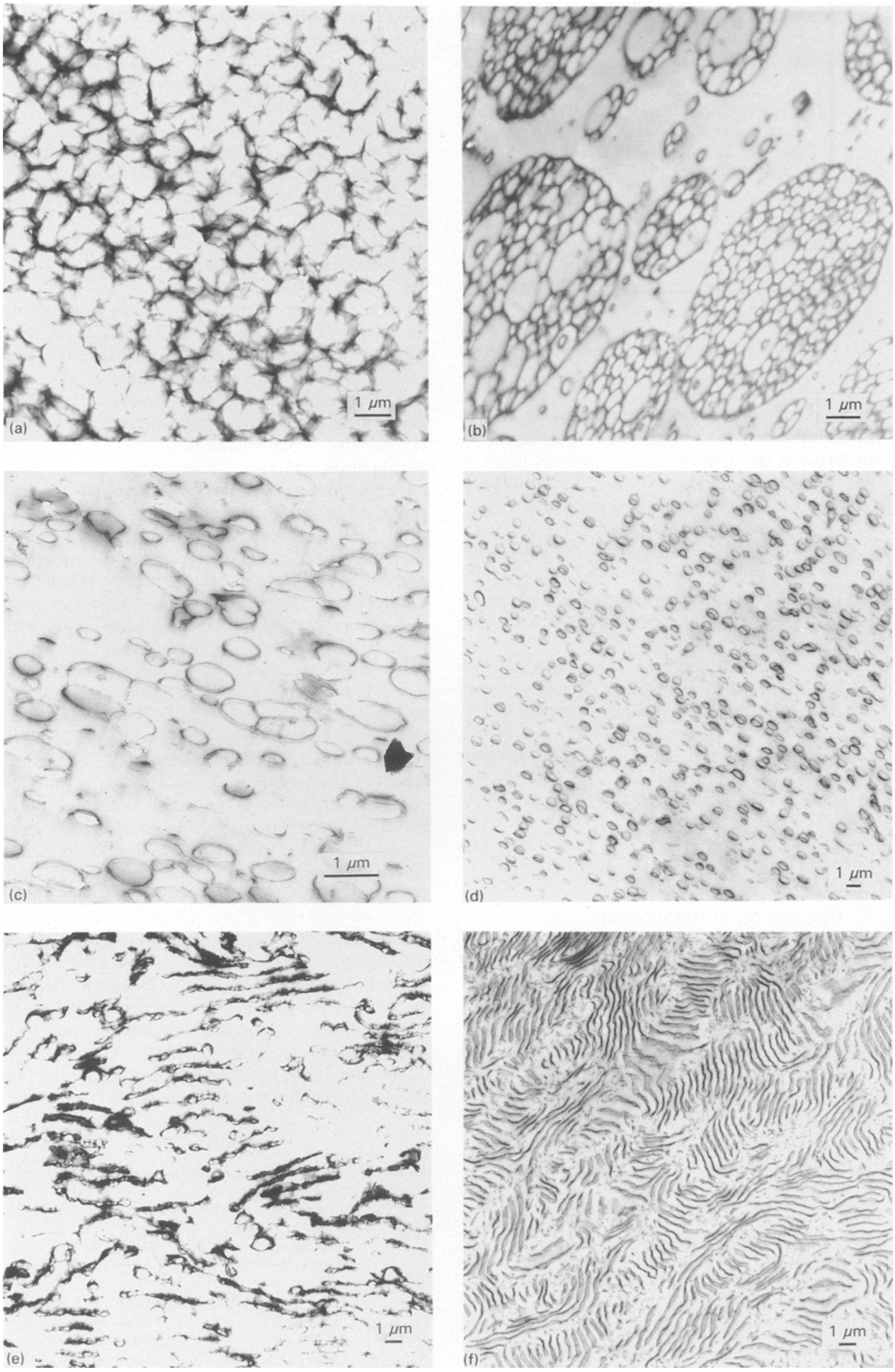

Figure 4 The microstructure of polybutadiene-reinforced poly(methylmethacrylate), A–F.

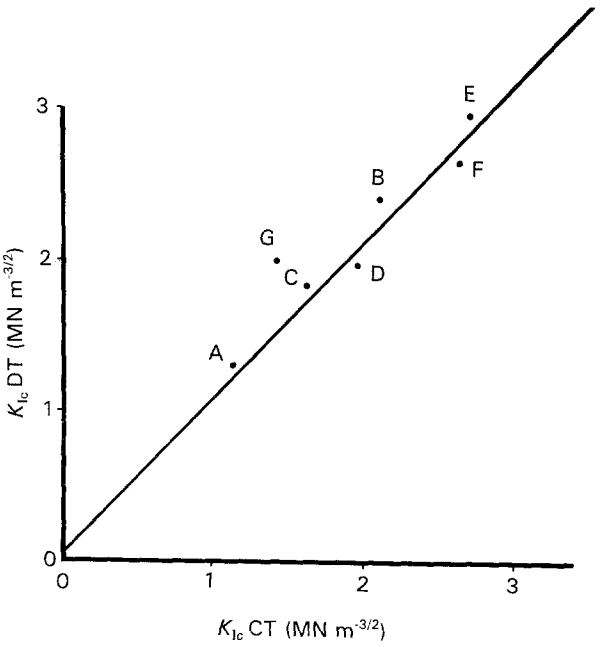

Figure 5 Correlation of fracture toughness data: plot of K_{IC} DT against K_{IC} CT. The good agreement between K_{IC} CT and K_{IC} DT indicates that the application of LEFM to these materials is valid.

TABLE II Stress intensity factor, K_{IC}, and strain energy release rate, G_{IC}, determined using the DT test

Material	K_{IC} (MN m$^{-3/2}$)	S.D. ($n = 5$)	G_{IC} (J m^{-2})	S.D. ($n = 5$)
A	2.21	0.22	5133	1024
B	1.85	0.18	4139	91
C	1.96	0.12	2592	236
D	2.94	0.08	3084	189
E	2.65	0.07	4199	162
F	2.02	0.11	2286	153
G	1.38	0.02	487	20

thick compact tension (CT) tests. There is a good correlation for the two sets of data with the exception of material A. However, the DT data give a value for the fracture toughness of approximately 10% (see Table II) higher than those from the CT tests. The reason for this is not clear, but the DT test has previously given higher values than the CT test [39]. In addition to the correlation of the fracture toughness data, there was no evidence in any of the materials except material A, of shear lips on the fracture surfaces, or of changes in the fracture morphology across the thickness of the specimens, that are indicative of a plane stress condition. The thicker 6 mm compact tension specimens all gave identical fracture toughness and toughness values to those obtained with the 3 mm thick specimens except for material A. Thus valid plane strain fracture toughness results were being obtained for all the materials except material A.

Neglecting material A, the fracture toughness, K_{IC}, values reach a maximum for material D with fine well-dispersed rubber particles with a core–shell microstructure. This type of morphology is that found in commercial samples of rubber-toughened acrylics (A1) and the results presented here suggest that this gives close to the optimum fracture toughness. It is worth noting that material E with a lamellar-type morphology also has a high fracture toughness only slightly below that of the core–shell microstructure.

The toughness, G_{IC}, values shown in Table II were surprising. The material that shows the greatest apparent toughness is material A, where the rubber is present as the continuous phase. The toughness appears to fall as the rubber particles become smaller and then rises again for very small particles, and as the morphology moves from a particle-type microstructure to a lamellar-type microstructure. As the lamellae become more pronounced, the toughness falls quite dramatically from 4199 J m^{-2} for material E to 2286 J m^{-2} for material F.

Fig. 6a–f show scanning electron micrographs of the fracture surfaces of the polybutadiene-reinforced materials. It is worth comparing these with the transmission electron micrographs, which were taken at approximately the same magnification. Material A (Fig. 6a) has undergone marked cavitation within the rubber phase and the high apparent toughness must arise from this cavitation mechanism. Fracture appears to have taken place either at the rubber poly(methylmethacrylate) interface, or within the rubber phase.

Cavitation is also seen in the large occluded particles of material B. In this material, fracture appears to have taken place through the poly(methylmethacrylate) glassy phase, including through the glassy inclusions within the rubber particles. In material C there appears to be a change in fracture mechanism with cavitation of the rubber phase, plus the glassy phase now appears to have undergone plastic shear. This process is more marked with material D, the fracture surface of which is similar to that found on commercial rubber-toughened acrylics which are also known to undergo cavitation and plastic shear [24] rather than the classical crazing process [17].

Material E (Fig. 6e with a lamellar-type microstructure) exhibits a totally different fracture morphology. The rubber lamellae, which are aligned in rows in the material appear to redirect the crack, resulting in a rough fracture surface and a large amount of surface area being created. This results in a very high toughness. The ability of the lamellae to redirect the propagating crack is clearly seen in the enlarged micrograph shown in Fig. 7. To the knowledge of the author, this type of toughening mechanism has not been observed before in rubber-toughened polymers. The fracture mechanism is directly analogous to that found in machineable glass-ceramics based on mica-type crystalline phases. Commercial ABS samples with this lamellar-type structure are also likely to undergo the same type of toughening mechanism. The fracture mechanism clearly results in G_{IC} being increased by almost ten-fold compared to the untoughened material. In material F, the polybutadiene lamellae do not enable such a marked ability to redirect the propagating crack. The reason for this is not clear at present and further work would be required to

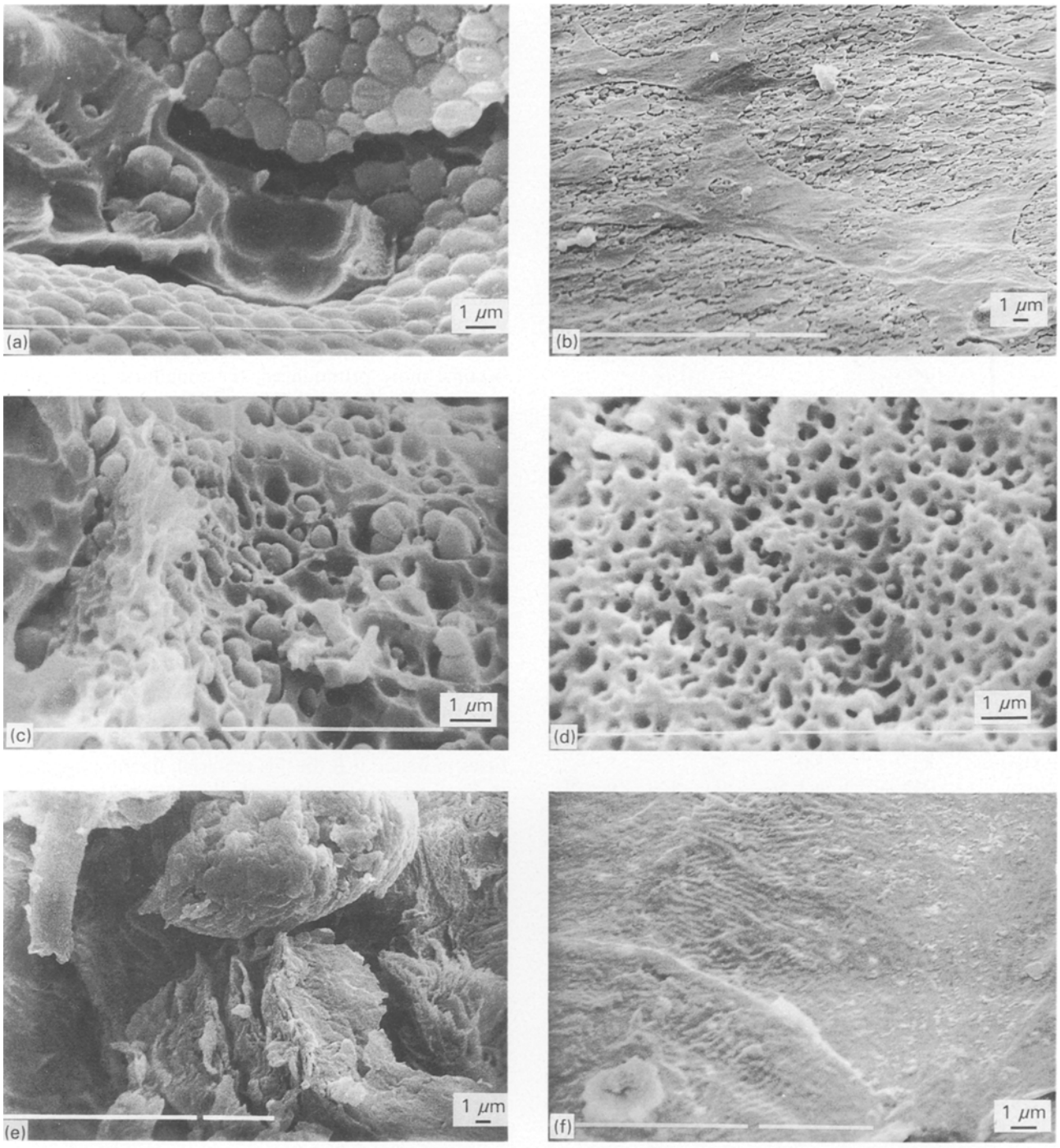

Figure 6 Scanning electron micrographs of the fracture surfaces of materials A–F.

determine the various parameters of the lamellae type microstructure that were important in determining the toughness. The unnotched fracture strengths of all the polybutadiene-reinforced materials (Table I) are all lower than the unreinforced material. The tensile edge of the fracture surfaces of the rubber-toughened materials all exhibited stress whitening. The most extensive stress whitening occurred with material A and it is thought that the stress whitening corresponds to cavitation of the polybutadiene phase. Because the rubber phase is the continuous phase in this material, the stress whitening can extend over a large volume of the sample. It is thought that the stress-whitened region acts as a large Griffith flaw through which subsequent crack propagation takes place in these materials. Thus the unnotched fracture strength of these materials depends on the fracture toughness and the size of the stress-whitened zone that forms prior to critical crack propagation.

Table III shows the calculated inherent Griffith flaw sizes. The untoughened material has a very small inherent flaw size. The inherent Griffith flaw size falls as the polybutadiene phase becomes increasingly well dispersed, reaching a minimum for material D with the core–shell microstructure before rising for the two lamellar-type morphologies.

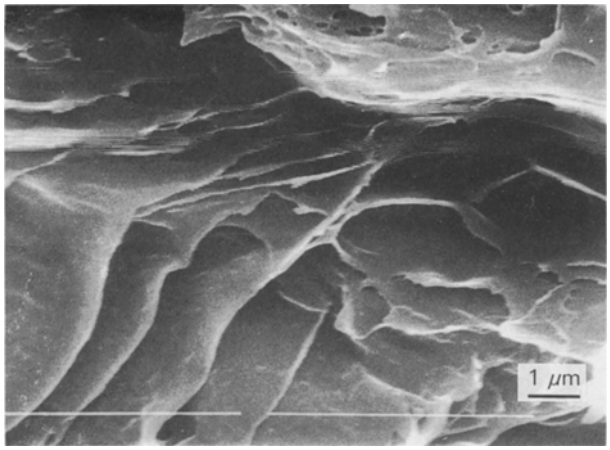

Figure 7 Rubber lamellae redirecting the crack-growth direction in material E.

TABLE III Inherent Griffith flaw sizes calculated from the DT test data

Material	a^* (mm)
A	0.853
B	0.731
C	0.414
D	0.371
E	0.436
F	0.297
G	0.044

4. Conclusions

1. Cavitation within the polybutadiene phase is the dominant mechanism for increasing the toughness of the continuous and particulate rubber morphologies studied. Crazing in the matrix was not observed in any of the materials, though this may be due to the presence of the cross-linking agent used in the preparation of these materials.

2. Plastic yielding in the matrix was an important mechanism in increasing the toughness of the material with the core–shell microstructure.

3. The toughening mechanism in lamellar-type rubber morphologies was different to that observed for the particulate morphologies and the toughness was increased as a result of the lamellae redirecting the propagating crack to produce a rough fracture surface.

4. The Young's modulus was highly dependent on the degree of dispersion of the polybutadiene phase within the poly(methylmethacrylate) phase.

5. Stress-whitened deformation zones formed prior to critical crack propagation in all the rubber-reinforced materials studied. Subsequent crack propagation took place through the stress-whitened zone, which probably acted as a Griffith flaw and served to reduce the unnotched fracture strength of these materials.

6. The highest fracture toughness was exhibited by the material with a core–shell microstructure that had both a high toughness and a high Young's modulus.

7. Rubber reinforcement is a practical method of improving the fracture resistance of both acrylic denture base polymers and acrylic bone cements.

References

1. M. S. BEYL and J. A. FRAUNHOFER, *Removable Prosthodontics* **46** (1981) 238.
2. A. S. HARGREAVES, *Br. Dent. J.* **126** (1969) 451.
3. F. A. WEBER and J. CHARNLEY, *J. B. Jt Surg.* **B57** (1975) 297.
4. T. A. GRUEN, G. M. McNIECE, H. C. AMSTATZ, *Clin. Orthop. Relat. Res.* **141** (1979) 17.
5. M. MARTENS, E. AERNOUDT, P. DEMEESTER, P. DUCHEYNE, J. C. MALIER, R. DELANGH and P. KESTELIJN, *Acta Orthop. Scand.* **45** (1974) 693.
6. M. PATERSON, P. FULFORD and R. DENHAM, *J. B. Jt Surg.* **B68** (1986) 392.
7. G. M. LEWIS, *J. Mater. Educ.* **11** (1989) 429.
8. B. WEIGHTMAN, M. A. R. FREEMAN, P. A. REVELL, M. BRADEN, B. E. J. ALBRECKTSSON and L. V. CARLSON, *J. Bone Jt Surg.* **69** (1987) 558.
9. L. M. JONCK and C. J. GROBBELAAR, *Clin. Mater.* **6** (1990) 323.
10. D. J. WOOD and R. G. HILL, *Biomaterials* **12** (1991) 164.
11. R. M. PILLIAR, R. BACKWELL, T. MacNAB and H. V. CAMERON, *J. Biomed. Mater. Res.* **10** (1976) 893.
12. T. M. WRIGHT and P. S. TRENT, *J. Mater. Sci.* **14** (1979) 503.
13. T. M. WRIGHT and R. P. ROBINSON, *ibid.* **17** (1982) 2463.
14. B. POURDEYHIMI, H. D. WAGNER and P. SCHWARTZ, *ibid.* **21** (1986) 4468.
15. A. J. BOWMAN and T. R. MANLEY, *Br. Dent. J.* **156** (1984) 57.
16. A. MURAKAMI, J. C. BEHIRI and W. BONFIELD, *J. Mater. Sci.* **23** (1988) 2029.
17. C. B. BUCKNALL, "Toughened Plastics" (Applied Science, London, 1977).
18. C. G. BRAGAW, *Adv. Chem. Ser.* **99** (1971) 86.
19. B. D. LAUTERWASSER and E. J. KRAMER, *Philos. Mag.* **394** (1979) 467.
20. A. M. DONALD and E. J. KRAMER, *J. Appl. Polym. Sci.* **27** (1982) 3729.
21. C. B. BUCKNALL and I. C. DRINKWATER, *J. Mater. Sci.* **8** (1973) 1800.
22. H. BREWER, F. HAAF and J. STABENBOW, *J. Macromol. Sci. Phys.* **B14** (1977) 387.
23. F. HAAF, H. BREWER and J. STABENBOW, *Angew Makromol. Chem.* **58/59** (1977) 95.
24. C. B. BUCKNALL, I. K. PARTRIDGE and M. V. WARD, *J. Mater. Sci.* **19** (1984) 2064.
25. A. M. DONALD and E. J. KRAMER, *ibid.* **17** (1982) 2351.
26. *Idem, ibid.* **17** (1982) 1765.
27. S. L. ROSEN, *Polym. Eng. Sci.* **7** (1967) 115.
28. L. NICOLAIS and M. MARKIS, *ibid.* **13** (1973) 469.
29. J. J. BENBOW and F. C. ROESLER, *Proc. Phys. Soc.* **B70** (1957) 201.
30. J. P. BERRY *J. Polym. Sci.* **50** (1961) 313.
31. A. VAN DER BOOGART and C. E. TURNER, *Trans. J. Plast. Inst.* **31** (1963) 109.
32. G. R. MARSHALL, L. E. CULVER and J. G. WILLIAMS, *J. Plast. Inst.* **36** (1968) 75.
33. S. KUNZ-DOUGLAS, P. W. R. BEAUMONT and M. F. ASHBY, *J. Mater. Sci.* **15** (1980) 1104.
34. K. NIKPUR and J. G. WILLIAMS, *ibid.* **14** (1979) 467.
35. R. J. FERGUSON, C. D. MARSHALL and J. G. WILLIAMS, *Polymer* **14** (1973) 451.
36. R. D. HOFFMAN and O. RICHMOND, *J. Appl. Phys.* **47** (1976) 4289.
37. J. A. KIES and B. J. CLARKE, in "Fracture", edited by P. L. Pratt (Chapman and Hall, London, 1969) p. 483.

38. BS 5447, "Plane Strain Fracture Toughness K_{IC} of Metallic Materials" (British Standards Institute, London, 1977).
39. R. G. HILL, J. F. BATES, T. T. LEWIS and N. REES, *Biomater.* **4** (1983) 112.
40. ASTMS D 790-71, "Standard Methods of Test for the Flexural Properties of Plastics" (American Society of Testing and Materials, Philadelphia, PA, 1971).
41. W. F. BROWN and J. E. STRAWLEY, "Plain Strain Crack Toughness Testing of High Strength Metallic Materials", ASTMS STP 410 (American Society of Testing and Materials, Philadelphia, PA, 1965) p. 13.
42. J. MILIOS, G. C. PAPANICOLAU and R. J. YOUNG, *J. Mater. Sci.* **21** (1986) 4281.

Received 7 September 1992
and accepted 10 November 1993